Pergamon

0277-5387(94)00400-5

Polyhedron Vol. 14, No. 1, pp. 11–23, 1995

0277-5387/95 $9.50+0.00

SYNTHESIS, STRUCTURE AND FLUXIONAL BEHAVIOR OF $[\eta^5\text{-}C_5H_3\text{-}1,3\text{-}(SiMe_2CH_2PPr^i_2)_2]ZrCl_{3-x}R_x$ (R = Me, CH_2Ph, $x = 0, 1, 3$)*

MICHAEL D. FRYZUK,† SHANE S. H. MAO, PAUL B. DUVAL and STEVEN J. RETTIG‡

Department of Chemistry, University of British Columbia, 2036 Main Mall, Vancouver, B.C., V6T 1Z1, Canada

Abstract—The addition of the potentially tridentate ligand $[P_2Cp]Li$ ($[P_2Cp]Li = (\eta^5\text{-}C_5H_3\text{-}1,3\text{-}(SiMe_2CH_2PPr^i_2)_2)Li$) to $ZrCl_4(THT)_2$ (THT = tetrahydrothiophene) generates $[P_2Cp]ZrCl_3$. The X-ray crystal structure of this compound is described; crystals are orthorhombic, space group $P2_12_12_1$ having $a = 14.282(2)$, $b = 15.877(3)$, and $c = 13.791(3)$ Å, $Z = 4$; the structure was solved by the Patterson method and was refined by full-matrix least-squares to $R = 0.032$ and $R_w = 0.027$ for 2907 reflections with $I \geqslant 3\sigma(I)$. The solution behavior of this compound is consistent with the solid state structure in that the phosphine arms of the ligand remain coordinated. Alkylation of $[P_2Cp]ZrCl_3$ generates the corresponding alkyl complexes $[P_2Cp]ZrCl_{3-x}R_x$ ($x = 1$ or 3). In solution $[P_2Cp]Zr(CH_2Ph)_3$ exists in a four-coordinate pseudo-tetrahedral geometry with the two phosphine arms dangling. However, at low temperatures the complexes $[P_2Cp]ZrCl_2(CH_2Ph)$ and $[P_2Cp]ZrMe_3$ exist as five-coordinate trigonal-bipyramidal structures with one phosphine coordinated and one phosphine uncoordinated. In these five-coordinate complexes, the coordinated phosphine exchanges with the uncoordinated phosphine via a dissociative pathway and/or an associative pathway depending on the number of hydrocarbyl substituents. The fluxional behavior of these complexes was studied by variable temperature $^{31}P\{^1H\}$, $^{13}C\{^1H\}$ and ^1H NMR spectroscopy, and activation parameters were estimated.

Early transition metal–alkyl complexes that contain cyclopentadienyl ancillary ligands have been implicated in many catalytic processes including Ziegler–Natta polymerization[1–7] and olefin oligomerization.[8,9] For example, group 4 complexes of the type, $(\eta^5\text{-}C_5H_5)_2ZrR_2$, can be converted to cations to generate extremely active, olefin polymerization catalysts.[2,4,5,10–21] Investigations have subsequently shown that modifying the cyclopentadienyl units can lead to catalysts that stereospecifically polymerize propylene to highly isotactic polypropylene.[6,7,22–27] A number of modifications have been examined and it is clear that the choice of the ancillary ligand is a key feature in catalyst development.[4,28,29]

For a number of years, our approach to ligand design has centered on the tridentate, mixed donor system **I** shown below:[30,31]

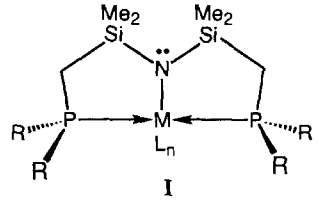

I

For early transition metal complexes, particularly groups 3 and 4, and the lanthanides, the amide portion of ligand **I** serves to anchor the ancillary

* Dedicated to Professor J. E. Bercaw on the occasion of his 50th birthday.

† Author to whom correspondence should be addressed.

‡ Professional Officer: UBC Crystallographic Service.

ligand encouraging the phosphines to bind to the metal and modulate its reactivity. However, two of the main drawbacks to this type of ligand system are the extreme hydrolytic instability of the NSi_2 unit in the ligand backbone and the inherent basicity of the amide linkage. In an effort to overcome these two limitations, we have developed a second generation ligand design in which the formally negatively-charged, basic amide donor has been replaced by a cyclopentadienyl unit as in **II**. The lower basicity of cyclopentadiene ($pK_a = 15$)[32] as compared to a disilylamine ($pK_a = 25.8$)[33] solves the basicity issue. As this second generation ligand incorporates carbon–silicon linkages in the backbone, the problem of hydrolytic instability of the ligand backbone is obviated.

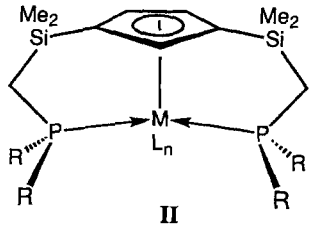

II

In this paper we describe our first efforts in the coordination chemistry of this second generation ligand using zirconium as the central metal.[34] The preparation of $[\eta^5\text{-}C_5H_3\text{-}1,3\text{-}(SiMe_2CH_2PPr^i_2)_2]ZrCl_3$ ($[P_2Cp]ZrCl_3$) is described along with a number of hydrocarbyl derivatives $[P_2Cp]ZrCl_{3-x}R_x$ (R = Me or CH_2Ph; $x = 1$ or 3). What emerges from this work is that phosphine coordination to the zirconium center becomes less prevalent and therefore more prone to dissociation as the number and size of the alkyl groups attached to zirconium increases. One of the consequences of facile phosphine dissociation is the observation of fluxional behavior which will be discussed.

RESULTS AND DISCUSSION

Synthesis and structure of $[P_2Cp]ZrCl_3$

Reaction of the ligand $[P_2Cp]Li$ with one equivalent of $ZrCl_4(THT)_2$ (THT = tetrahydrothiophene) in toluene solution generates the monoligand complex $[P_2Cp]ZrCl_3$ (**1**) in nearly quantitative yield as pale yellow, air- and moisture-sensitive crystals. The use of a non-coordinating solvent such as toluene in the preparation of **1** is crucial. If the reaction is performed in THF, an oily yellow material is obtained that shows new ligand resonances distinct from **1** and also resonances due to unreacted $[P_2Cp]Li$ by ^1H and $^{31}P\{^1H\}$ NMR spectroscopy; we assign the identity of these new resonances as being due to the bis(ligand) derivative $[P_2Cp]_2ZrCl_2$. Additional evidence for this conclusion comes from the reaction of authentic monoligand complex **1** with an additional equivalent of $[P_2Cp]Li$ in THF to produce the identical material. The NMR spectroscopic parameters of the monoligand complex **1** are simple; the $^{31}P\{^1H\}$ NMR spectrum shows a singlet at 10.7 ppm consistent with equivalent phosphorus donors, while the ^1H NMR spectrum displays two cyclopentadienyl proton resonances in the ratio of 1 : 2, and appropriate peaks for the methylene (PCH_2Si), silylmethyl ($Si(CH_3)_2$) and isopropyl ($PCH(CH_3)_2$) protons in a complex with C_s symmetry.

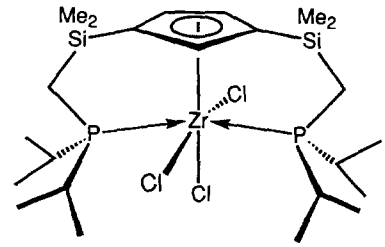

1

One can speculate on the importance of the reaction solvent by assuming that the first step involves the metathesis of the chloride in $ZrCl_4(THT)_2$ by $[P_2Cp]Li$ and formation of $[P_2Cp]ZrCl_3(THT)_2$ having both phosphine arms dangling. In toluene, the THT ligands are replaced by the phosphine donors to generate **1** in a faster step than further reaction with $[P_2Cp]Li$; however, in THF solvent, the metathesis presumably generates a species having coordinated THF and dangling phosphines, that is, $[P_2Cp]ZrCl_3(THF)_2$, and this species can undergo further reaction with $[P_2Cp]Li$ to generate the bis(ligand) material, $[P_2Cp]_2ZrCl_2$, before the phosphines displace the coordinated THF.

The molecular structure of **1** (Fig. 1, Tables 1 and 2) is best described as a distorted, quasi-octahedron assuming that the cyclopentadienyl unit occupies one site. This geometry is distorted since both the P1—Zr—P2 angle of 159.53(4)° and the Cl1—Zr—Cl2 angle of 160.61(5)°, are both approximately 20° away from the ideal linear 180°. In addition, both of these angles bend away from the cyclopentadienyl unit. By way of comparison, the structures and molecular parameters of $ZrCl_3[N(SiMe_2CH_2PPr^i_2)_2]$,[35] the analogous complex with one amidodiphosphine ligand, and $(\eta^5\text{-}C_5H_5)ZrCl_3$, the mono(cyclopentadienyl) complex,[36] are informative. The Zr—P bond distances in **1** of 2.897(1) and 2.871(1) Å are considerably longer than those found in $ZrCl_3[N(Si$

Table 1. Selected bond lengths for $[P_2Cp]ZrCl_3$ (**1**)

Bond	Length (Å)	Bond	Length (Å)	Bond	Length (Å)
Zr—C11	2.489(1)	Zr—Cp	2.260(5)	C1—C2	1.409(6)
Zr—C12	2.490(1)	Si1—C1	1.874(4)	C1—C5	1.424(7)
Zr—C13	2.529(1)	Si1—C6	1.873(6)	C2—C3	1.424(7)
Zr—P1	2.897(1)	Si2—C3	1.863(5)	C3—C4	1.422(6)
Zr—P2	2.871(1)	Si2—C7	1.875(5)	C4—C5	1.397(7)

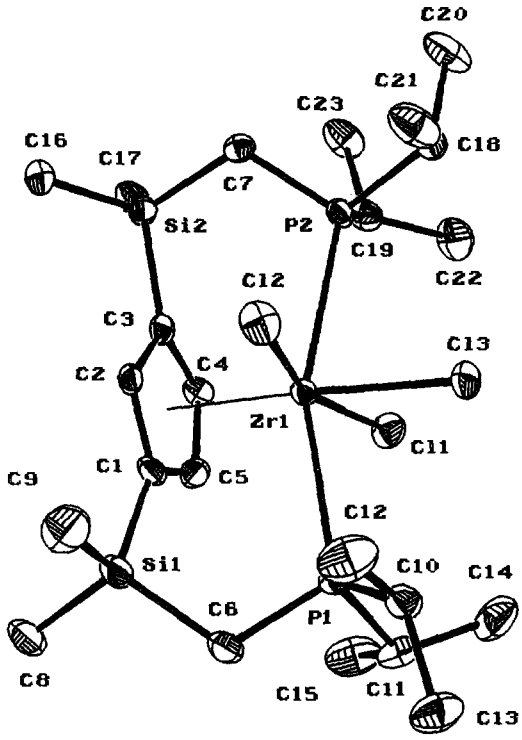

Fig. 1. Molecular structure and numbering diagram for $[P_2Cp]ZrCl_3$ (**1**).

Table 2. Selected bond angles for $[P_2Cp]ZrCl_3$ (**1**)

Bonds	Angle (°)	Bonds	Angle (°)
C11—Zr—C12	160.61(5)	C11—Zr—Cp	98.34
C11—Zr—C13	80.79(5)	C12—Zr—Cp	98.98
C12—Zr—C13	81.19(5)	C13—Zr—Cp	177.50
C11—Zr—P1	88.57(5)	P1—Zr—P2	159.53(4)
C11—Zr—P2	85.23(4)	P1—Zr—Cp	99.18
C12—Zr—P1	94.74(5)	P2—Zr—Cp	101.07
C12—Zr—P2	85.07(4)		
C13—Zr—P1	78.32(4)		
C13—Zr—P2	81.43(4)		

$Me_2CH_2PPr^i_2)_2]$, 2.7833(12) and 2.7645(12) Å. In addition, the phosphine arms of the amido-diphosphine ligand are pulled back towards the amide unit such that the P—Zr—P atoms subtend an angle of 159.38(4)°, virtually identical to the analogous angle found in **1** but, as already mentioned, the latter arms are bent away from the cyclopentadienyl anchor. The Zr—Cp(centroid) distance in **1** is 2.260(5) Å and is longer than that found in polymeric $(\eta^5\text{-}C_5H_5)ZrCl_3$ (Zr—Cp(centroid) is 2.196 Å). In **1**, the Zr—Cl bond distances range from 2.489(1) to 2.529(1) Å and are somewhat longer than those found in both $ZrCl_3[N(SiMe_2CH_2PPr^i_2)_2]$ and $(\eta^5\text{-}C_5H_5)ZrCl_3$.

In solution, the fact that the $^{31}P\{^1H\}$, $^{13}C\{^1H\}$ and ^1H NMR spectra are consistent with a geometry having C_s symmetry suggests strongly that the solution and solid state structures are virtually identical. It is also important to note that the NMR spectra are invariant with changes in temperature which implies that the phosphine arms of **1** are not undergoing any detectable exchange process. An interesting sidebar to the ^1H NMR spectrum of **1** is the observation that the resonance of the unique proton of the cyclopentadienyl ring (hydrogen attached to Cp2) shifts from 6.0 ppm in $[P_2Cp]Li$ to 7.3 ppm in $[P_2Cp]ZrCl_3$, while the resonance owing to the remaining two protons (hydrogens attached to Cp4 and Cp5) remain at the same position of 6.4 ppm. This may be owing to a weak interaction between that single proton and chloride on the same side (C12). The distance between these two atoms as measured from the X-ray crystal structure is 2.7 Å, which is significantly shorter than the van der Waals distance (3.0 Å).[37]

Synthesis of hydrocarbyl derivatives $[P_2Cp]ZrCl_{3-x}R_x$

The preparation of one monoalkyl ($R = CH_2Ph$, $x = 1$) and two trialkyl ($R = CH_2Ph$ and CH_3,

$x = 3$) complexes is described; the noticeably absent dialkyls will be discussed separately in the context of their transformation to alkylidene derivatives.[34] Addition of 1.5 equivalents of $Mg(CH_2Ph)_2(THF)_2$ to $[P_2Cp]ZrCl_3$ generates the tribenzyl derivative $[P_2Cp]Zr(CH_2Ph)_3$ (**2**) as shown in eq. (1).

$$[P_2Cp]ZrCl_3 + 3/2\,Mg(CH_2Ph)_2(THF)_2 \quad \mathbf{1}$$

$$\xrightarrow[(-3/2\,MgCl_2)]{\text{toluene}\ -78^\circ C} [P_2Cp]Zr(CH_2Ph)_3 \quad \mathbf{2} \qquad (1)$$

The product is extremely soluble in pentane and can only be isolated as a yellowish air- and moisture-sensitive, thermally-stable oil.

^1H and $^{13}C\{^1H\}$ and $^{31}P\{^1H\}$ NMR spectroscopic data are consistent with the presence of three benzyl groups and one P_2Cp moiety per zirconium. At ambient temperatures, a singlet in the $^{31}P\{^1H\}$ NMR spectrum is observed at -5.2 ppm close to the frequency of the free ligand (-7.0 for $[P_2Cp]H$) and is indicative of two uncoordinated phosphine donors. In both the ^1H and $^{13}C\{^1H\}$ NMR spectra, all three benzyl groups are equivalent at all temperatures; moreover, the protons and the carbon of the benzyl CH_2 groups appear as singlets in the respective ^1H and $^{13}C\{^1H\}$ NMR spectra. The fact that no coupling to ^{31}P is observed is further evidence that the phosphine arms of the ligand are dangling in this complex. The spectroscopic data strongly indicate a pseudo-tetrahedral geometry as the solution structure.

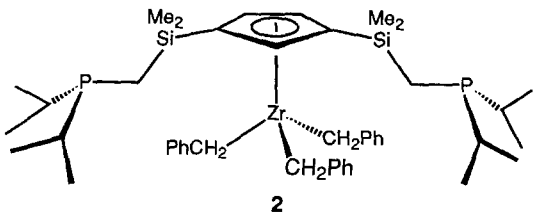

2

Even at low temperatures ^1H, $^{31}P\{^1H\}$ and $^{13}C\{^1H\}$ NMR spectroscopic studies failed to provide any evidence of phosphine coordination.

Addition of 0.5 equivalents of $Mg(CH_2Ph)_2(THF)_2$ to $[P_2Cp]ZrCl_3$ (**1**) generates the monobenzyl derivative $[P_2Cp]ZrCl_2(CH_2Ph)$ (**3**) as shown in eq. (2).

$$[P_2Cp]ZrCl_3 + 1/2\,Mg(CH_2Ph)_2(THF)_2 \quad \mathbf{1}$$

$$\xrightarrow[(-1/2\,MgCl_2)]{\text{toluene}\ -78^\circ C} [P_2Cp]ZrCl_2(CH_2Ph) \quad \mathbf{3} \qquad (2)$$

Again, attempts to obtain crystals of the monobenzyl derivative **3** were thwarted by its extreme solubility even in cold pentane ($-78^\circ C$); the product is isolated as a yellowish air- and moisture-sensitive, thermally-stable oil.

By accurate integration of the ^1H NMR spectrum, only one benzyl group per $[P_2Cp]$ unit is observed. At $-10^\circ C$, $^{31}P\{^1H\}$ NMR spectrum shows two singlets at 14.2 and -6.9 ppm which are in a ratio of 1 : 1. The lowfield peak at 14.2 ppm is owing to coordinated phosphine since it occurs close to that found for $[P_2Cp]ZrCl_3$ ($^{31}P\{^1H\}$ NMR spectrum of **1** shows a singlet at 10.7 ppm); the position of this resonance is not temperature dependent although the peak does broaden and coalesce at higher temperatures as discussed below. The position of the highfield peak at -6.9 ppm is somewhat temperature dependent and is observed close to the resonance of the free phosphine as found in $[P_2Cp]H$ (-7 ppm at $-10^\circ C$); in fact, the temperature dependence of this latter peak mirrors the temperature dependence of the $^{31}P\{^1H\}$ NMR peak of $[P_2Cp]H$. As the temperature is raised, these two singlets in the $^{31}P\{^1H\}$ NMR spectrum coalesce at $30.5^\circ C$ into a broad singlet at 5.8 ppm which sharpens at higher temperatures. At ambient temperature, the $^{13}C\{^1H\}$ spectrum shows a triplet for the benzylic carbon (CH_2) owing to coupling to two equivalent ^{31}P nuclei.

Based on this variable temperature spectroscopic data, the solution structure of the monobenzyl derivative is a pseudo five-coordinate geometry in the slow exchange limit.

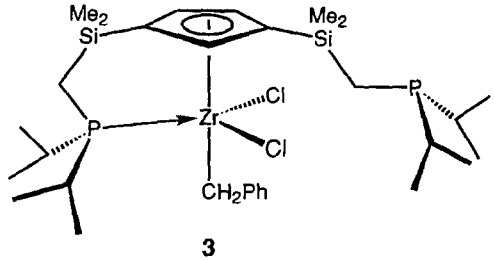

3

At higher temperatures, one can observe by $^{31}P\{^1H\}$ NMR spectroscopy the two phosphine arms in this five-coordinate species undergoing rapid exchange. Simulation of the temperature dependent $^{31}P\{^1H\}$ NMR spectra by NMR line shape analysis (DNMR-5) gave the following activation parameters from the calculated rate constants (Table 3, Fig. 2): $\Delta H^\ddagger = 8.8$ kcal mol^{-1}, $\Delta S^\ddagger = -13.1$ cal mol^{-1} K^{-1}.

The negative entropy of activation for this process is consistent with a transition state that is pseudo-six-coordinate, in other words, phosphine

Table 3. Rate constants of phosphine exchange for $[P_2Cp]ZrCl_2(CH_2Ph)$ (**3**) as obtained from line shape analysis using DNMR-5

T(°C)	−18.4	−8.4	1.9	12.1	22.4	30.5	40.5	50.5	60.5	70.4
k	200	400	800	1500	2500	4000	6500	11000	16000	24000

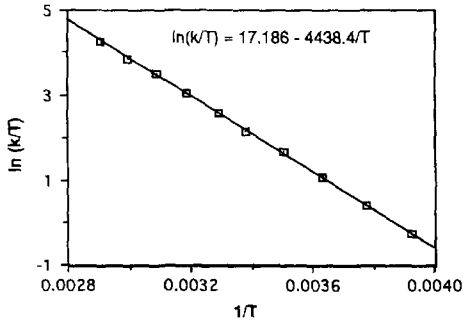

Fig. 2. Eyring plot of ln (k/T) *versus* $1/T$ for the complex $[P_2Cp]ZrCl_2(CH_2Ph)$ (**3**) using the equation $k = (k_BT/h)\exp(-\Delta G‡/RT) = (k_BT/h)\exp((T\Delta S‡ - \Delta H‡)/RT)$; the rate constants and temperatures are taken directly from Table 3.

exchange occurs via an associative pathway. Presumably, the transition state for this exchange in **3** has a structure similar to the starting monoligand complex **1**.

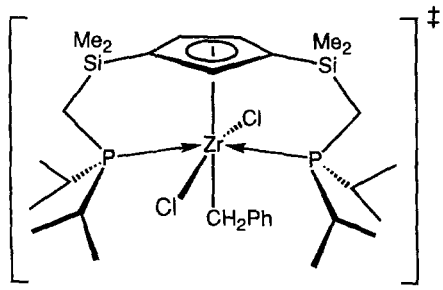

To examine the effect of the size of the hydrocarbyl substituent, the starting monoligand complex **1** was methylated; addition of three equivalents of $Mg(CH_3)Br$ to $[P_2Cp]ZrCl_3$ generates the trimethyl derivative $[P_2Cp]Zr(CH_3)_3$ (**4**) as shown in eq. (3).

$$[P_2Cp]ZrCl_3 + 3Mg(CH_3)Br \xrightarrow[(-3MgClBr)]{\text{toluene}\ -78°C} [P_2Cp]Zr(CH_3)_3 \quad (3)$$

1 → **4**

Because the product is extremely soluble in pentane, it could only be isolated as a yellowish air- and moisture-sensitive, slightly impure, thermally-stable oil; its stability is in marked contrast to the reported thermal lability of the related $Cp^*Zr(CH_3)_3$.[38] The trimethyl derivative **4** can also be synthesized from the reaction of $[P_2Cp]ZrCl_3$ and three equivalents MeLi. However, this reaction is quite sensitive to reaction stoichiometry; if a slight excess of MeLi is added at −78°C and the solution warmed up to ambient temperature, decomposition of the entire reaction mixture is complete in a few minutes. One of the reaction products detected in the resultant mixture is $[P_2Cp]Li$. Adding even 0.1 equivalents of MeLi to **4** induces the decomposition process. Presumably, the trimethyl complex **4** reacts with an additional equivalent of MeLi to generate $[P_2Cp]Li$ and the tetramethyl derivative $Zr(CH_3)_4$ which is a catalyst for the decomposition of $[P_2Cp]Zr(CH_3)_3$.

The NMR spectroscopic parameters for this trimethyl derivative are simple. At ambient temperature a singlet at 2.3 ppm in $^{31}P\{^1H\}$ NMR spectrum is observed, indicative of equivalent phosphine donors. The methyl groups directly attached to zirconium appear as one triplet in the ^1H NMR spectrum and one triplet at 42.7 ppm in the $^{13}C\{^1H\}$ NMR spectrum. In addition, the ligand backbone resonances are also very simple giving rise to a singlet for the silyl methyl protons and a doublet for the methylene hydrogens. As the temperature is lowered, these simple NMR spectra broaden and become more complicated. For example, at −78°C the $^{31}P\{^1H\}$ NMR spectrum of **4** shows two singlets at 9.8 and −9.7 ppm in a ratio of 1 : 1 (Fig. 3). This behavior is virtually identical to the monobenzyl derivative **3** except that the chemical shift of the dangling phosphine resonance is at slightly higher field, again due to the temperature dependence of chemical shift of this particular resonance (at −80°C, $[P_2Cp]H$ shows a peak at −9.0 ppm). At room temperature in the ^1H NMR spectrum, the peaks owing to the cyclopentadienyl protons appear as a triplet at 6.42 ppm owing to the unique proton (Cp2—H) and a doublet at 6.7 ppm due to the remaining equivalent protons (Cp4—H and Cp5—H). As the temperature is lowered, the triplet at 6.42 ppm broadens slightly but remains unchanged; however, the doublet at 6.7 ppm broadens and decoalesces until finally, at −80°C, there are two resonances at 6.9 and 6.4 ppm. The low tem-

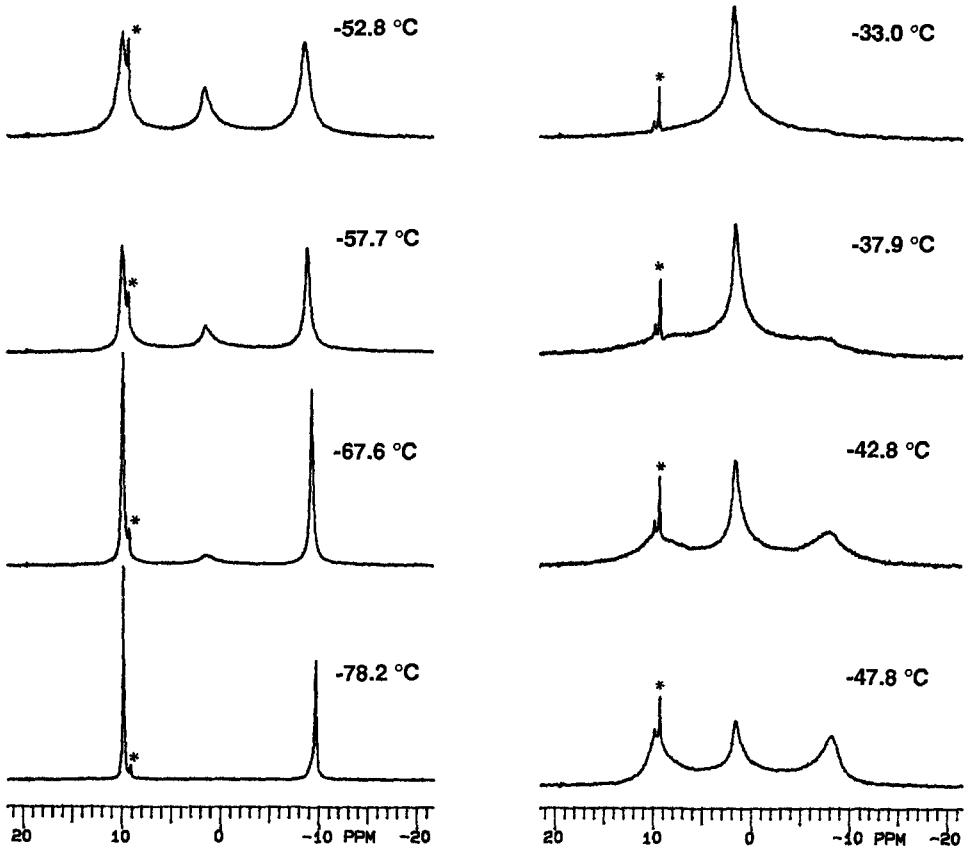

Fig. 3. Variable temperature $^{31}P\{^1H\}$ NMR spectra of $[P_2Cp]Zr(CH_3)_3$ (**4**); a minor unknown impurity is shown with an asterisk.

perature $^{13}C\{^1H\}$ NMR spectrum of **4** shows three methyl carbon resonances at approximately 44.2, 44.0 and 41.0 ppm (only one triplet at ambient temperature), three cyclopentadienyl carbon resonances (two resonances at ambient temperature); for completeness, the ipso carbons, Cp1 and Cp3, are not observed at low temperature at these concentrations. All of this NMR data indicate that a five-coordinated species is present at low temperature with one phosphine arm coordinated to zirconium and the other arm dangling, identical to that suggested above for the monobenzyl complex **3** at low temperature. A reasonable structure is shown below:

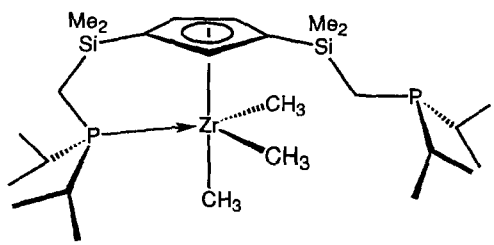

4

In the low temperature limit this particular geometry is consistent with all of the spectral data since it satisfies the requirement that the phosphine donors be inequivalent and that there are three types of zirconium–methyl carbon resonances in the $^{13}C\{^1H\}$ NMR spectrum.

It is tempting to ascribe the process that exchanges the phosphine donors and the methyl environments as being similar to that already suggested for the monobenzyl complex **3**, that is, an associative process whereby the dangling phosphine arms coordinates to generate a pseudooctahedral transition state. However, as will be discussed below, some of the features of the variable temperature $^{31}P\{^1H\}$ NMR spectra (Fig. 3) are not consistent with this straightforward interpretation.

As already mentioned, in the slow exchange limit (below $-78°C$) two singlets due to coordinated and uncoordinated phosphine donors are observed in the $^{31}P\{^1H\}$ NMR spectrum of **4** (see Fig. 3). However, as the temperature is raised, rather than observe simple coalescence of these two peaks, another singlet at approx. 1.6 ppm appears and its intensity increases with the increase in temperature.

Table 4. Rate constants of phosphine exchange for $[P_2Cp]Zr(CH_3)_3$ (**4**) as obtained from line shape analysis using DNMR-5

T(°C)	−78.2	−67.6	−57.7	−52.8	−47.8	−42.8	−37.9
k	10	50	300	600	1050	2050	4000

At the same time that this singlet's intensity is increasing, the original two singlet resonances begin to broaden and at approx. −37°C coalesce into this singlet at 1.6 ppm; this peak's chemical shift changes slightly with temperature until at ambient temperature it is measured at 2.3 ppm. The ^1H and $^{13}C\{^1H\}$ NMR spectra also show the corresponding changes, although less clearly.

One possible interpretation of this spectroscopic data is as follows: the trimethyl actually exists as two complexes in equilibrium, one of which is the five-coordinate derivative **4** and is favored at low temperatures and there is another species that persists at higher temperatures. The nature of the high temperature species will be discussed below. However, it is important to point out that both species are undergoing independent fluxional processes having coincident $^{31}P\{^1H\}$ NMR spectral characteristics.

In an attempt to quantify and differentiate these two processes, the $^{31}P\{^1H\}$ NMR spectral data were simulated by DNMR-5 (Table 4 and Fig. 4). Owing to limitations in this type of program, only the coalescence of the two singlet peaks owing to **4** in the low temperature $^{31}P\{^1H\}$ NMR spectra shown in Fig. 3 could be analyzed. An Eyring plot of the resultant rate constant data generates the following kinetic parameters: $\Delta H‡ = 13.2$ kcal mol^{-1} and $\Delta S‡ = 14.6$ cal mol^{-1} K^{-1}, from which $\Delta G‡ = 9.8$ kcal mol^{-1} at $T_c = -37$°C. What is intriguing is that $\Delta S‡$ is positive indicating that this exchange goes through a less ordered transition state than the five-coordinate, low temperature limiting structure; in other words, these parameters are most consistent with the dissociative pathway of exchange. A possible transition state for exchange of the phosphine donors is shown below as **4-D$_{pl}$**.

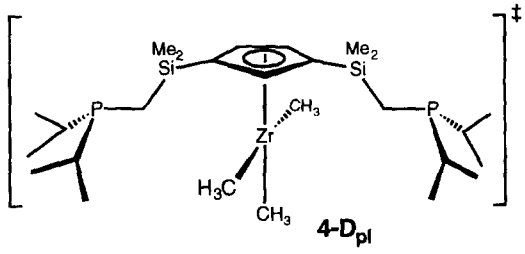

4-D$_{pl}$

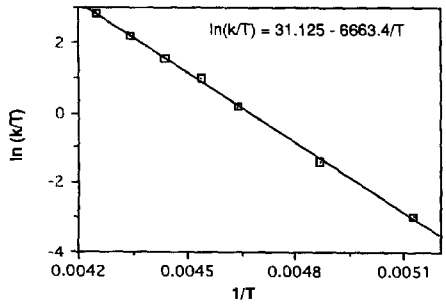

Fig. 4. Eyring plot of ln (k/T) *versus* $1/T$ for the complex $[P_2Cp]Zr(CH_3)_3$ (**4**) using the equation $k = (k_BT/h)\exp(-\Delta G‡/RT) = (k_BT/h)\exp((T\Delta S‡ - \Delta H‡)/RT)$; the rate constants and temperatures are taken directly from Table 4.

As already mentioned, in the variable temperature $^{31}P\{^1H\}$ NMR spectra, the appearance of the singlet at approximately 1.6 ppm above about −70°C but before coalescence of the singlet peaks owing to *dissociative* exchange of coordinated and uncoordinated phosphines suggests that there is another species present in equilibrium with the five-coordinate complex **4**. Integration of the variable temperature $^{31}P\{^1H\}$ NMR spectra between −68°C and −43°C did show that the two peaks owing to the five-coordinate complex **4** did decrease in intensity while the singlet at approximately 1.6 ppm increased; with the assumption of just two species in equilibrium, we were able to calculate equilibrium constants as a function of temperature and then plot them using the van't Hoff equation. The data are given in Table 5 and the plot is shown in Fig. 5; from this plot, values of $\Delta H° = 6.2 \pm 1.0$ kcal mol^{-1} and $\Delta S° = 25 \pm 10$ cal mol^{-1} K^{-1} were determined; the errors were estimated from different runs and indicate reproducibility.

We speculate that the two species shown in eq. (4) are involved in the equilibrium. The five-coordinate derivative **4** shown on the left-hand side of the equilibrium is favored at low temperatures while at higher temperatures the species labeled **4-A** predominates; this latter species has both phosphines coordinated to the zirconium center, however, we suggest that the phosphines are only weakly associated with the metal center. The main reason for this formulation is the $^{31}P\{^1H\}$ NMR spectrum wherein

Table 5. Equilibrium data for the two trimethyl complexes in equilibrium. The data were taken from the $^{31}P\{^{1}H\}$ NMR spectra shown in Fig. 3 at the indicated temperatures

T(°C)	−67.6	−62.7	−57.7	−52.8	−47.8	−42.8
k	0.078	0.113	0.176	0.202	0.305	0.409

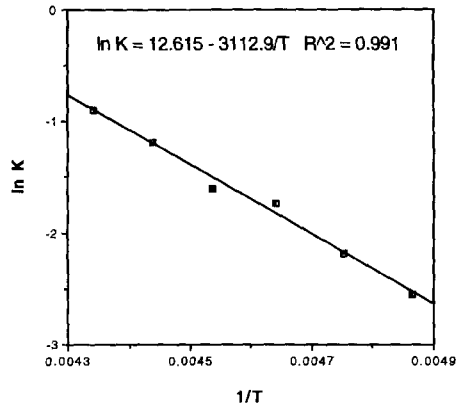

Fig. 5. A van't Hoff plot of the $^{31}P\{^{1}H\}$ NMR spectral data for the equilibrium shown in eq. (4); from this plot values of $\Delta H^{\circ} = 6.2 \pm 1.0$ kcal mol^{-1} and $\Delta S^{\circ} = 25 \pm 10$ cal mol^{-1} K^{-1} were calculated.

there is a single line owing to rapidly exchanging phosphine donors (see below) indicative of some degree of coordination.

sociative process for **4**; in other words, when the dissociative pathway is undergoing slow exchange at −78°C, the corresponding process for phosphine exchange in **4-A** is just at coalescence.

In Scheme 1, these two exchange processes for **4** and **4-A** are shown with the appropriate transition states **4-D$_{pl}$** and **4-D$_{tet}$** indicated. In the low temperature regime, **4** undergoes a dissociative process (on the basis of the positive $\Delta S\ddagger$) via the transition state **4-D$_{pl}$** with a barrier of $\Delta G\ddagger = 9.3$ kcal mol^{-1}. Overlaid on this process is the equilibrium involving **4-A** for which we propose weakly-bound phosphines undergoing fast dissociative exchange via **4-D$_{tet}$**. In light of the thermodynamic data, this proposal is somewhat counterintuitive since **4-A** would appear to be more ordered than **4**; however, if both phosphine ligands are only weakly bound there may be additional degrees of freedom that could account for the rather large, positive ΔS° term. To further add to the uncertainty, it should be noted again that there are large error bars in the thermodynamic parameters owing to the difficulty in making accu-

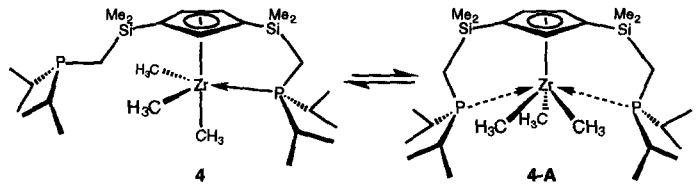

Line shape analysis of the fluxional process that exchanges the phosphine donors of **4-A** was not possible because the data are rather limited. However, an estimate for $\Delta G\ddagger$ of 7.9 kcal mol^{-1} could be made by using the usual formula[39] and the following assumptions: the coalescence temperature is −78°C and the peak separation, $\Delta\nu_c$, is 2370 Hz (difference between the $^{31}P\{^{1}H\}$ NMR peaks at 9.8 and −9.7 ppm at 121.421 MHz). These assumptions are based on the notion that the fluxional process for **4-A** is a lower energy process than the dissociative pathway mentioned above for **4** (via **4-D$_{pl}$**) since the appearance of the singlet at 1.6 ppm at approximately −60°C owing to the averaged phosphine environments of **4-A** occurs before coalescence of the peaks due to the dis-

rate integration of the $^{31}P\{^{1}H\}$ NMR spectra. Another possible species that could be in equilibrium with **4** is the proposed transition state for the higher energy process, **4-D$_{tet}$** shown in Scheme 1. This would be more consistent with the thermodynamic data because it could account for the large ΔS° term; however, such a species should give rise to a $^{31}P\{^{1}H\}$ NMR chemical shift close to that of an uncoordinated phosphine and for this reason we favor the loosely bound derivative **4-A**. It should also be noted that all of our suggestions up to this point rely on the results of the plot of the rate constants obtained from the simulation of the variable temperature $^{31}P\{^{1}H\}$ NMR spectra of the higher energy process involving **4**, in particular, the fact that $\Delta S\ddagger$ is positive, since this is the key piece

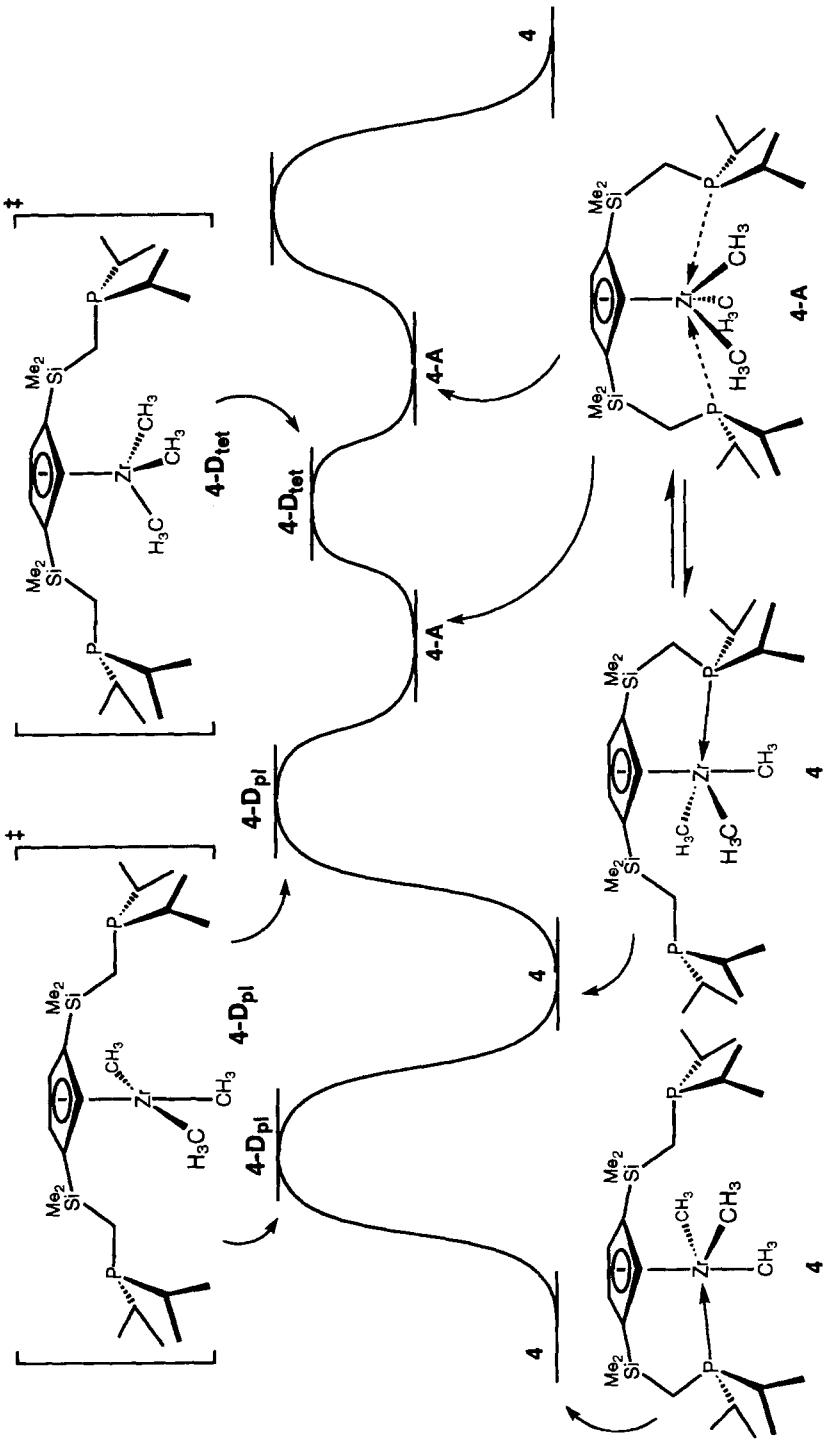

Scheme 1.

of evidence that is consistent with that particular dissociative process. Because the accuracy of the simulations was determined by visual comparison, this is a source of some concern. However, as shown in Table 6, determination of activation free energies $\Delta G\ddagger$ from peak separations and T_c values using low temperature ^1H NMR and $^{13}C\{^1H\}$ NMR spectra gives values of $\Delta G\ddagger = 9.8 \pm 0.1$ kcal mol^{-1} which is comparable to that from the simulation data. In addition, determining coalescence temperatures is not without error; for example, an overestimate of the error of determining the coalescence temperature of ± 5 K would lead to the error in $\Delta G\ddagger$ being approximately 0.2 kcal mol^{-1} at most.

The fluxional processes that are displayed by the series of complexes $[P_2Cp]ZrCl_{3-x}R_x$ depend on the extent of hydrocarbyl substitution. For the starting trichloride complex **1** ($x = 0$), the structure is rigid on the NMR time scale and the phosphorus donors are observed to be strongly bound to the zirconium center. However, as hydrocarbyl substituents are introduced, the phosphine ligands bind more weakly and as a consequence the complex becomes fluxional. For the tribenzyl derivative **2**, the phosphine donors remain uncoordinated over all temperatures studied and the equivalent benzyl groups arise from simple rotation of the $[P_2Cp]$ unit around the zirconium-centroid axis. For the monobenzyl complex **3**, only one phosphorus ligand binds in the low temperature limiting structure but exchange occurs via an associative mechanism. The most complicated solution behavior is found for the trimethyl complex **4**. In this case, an equilibrium between two independent processes is suggested to be operative to explain the NMR spectral data: at very low temperatures, a loosely bound six-coordinate species **4-A** undergoes a low energy dissociative process, and as the temperature is raised, another dissociative pathway also contributes to the exchange. In contrast, the related trimethyl derivative, $Zr(CH_3)_3[N(SiMe_2CH_2PPr^i_2)_2]$, which contains the amidodiphosphine ligand **I**, undergoes just associative exchange.[41]

A rationale that is consistent with all this data is that the electronegative chloride ligands render the zirconium center electropositive and enhance phosphine binding. As the chlorides are successively replaced by alkyl substituents, the zirconium center becomes less electropositive because of the electron-donating ability of hydrocarbyl groups; this in turn reduces the tendency for the phosphine donors to bind to the metal center. And there is also the steric requirements of the various ligands to consider since the chloride ligands are less bulky than methyl groups and thus do not impede access to the zirconium center. In the case of the tribenzyl derivative **3**, the presence of three very bulky hydrocarbyl groups do not allow any phosphine binding. For the trimethyl complex **4**, there exists a subtle balance of electronic and steric effects such that both dissociative and associative exchange of phosphine donors are observed.

Table 6. Calculation of exchange rate constants

Data from	$^{31}P\{^1H\}^a$	$^1H^b$	$^{13}C\{^1H\}^b$	$^{13}C\{^1H\}^b$
T_c (K)	236	215	215	215
$\Delta\nu_c$ (Hz)	2149.2	148.2	259.1	232.8
$\Delta G\ddagger$ (kcal mol^{-1})	9.7	9.9	9.7	9.8

$$k_c = \pi\Delta\nu_c/\sqrt{2} \quad \text{and} \quad \Delta G\ddagger = -RT_c \ln\left(\frac{\pi\Delta\nu_c}{\sqrt{2}k_B T_c}\right)$$

where R is the gas constant, T_c is the temperature of coalescence, h is Planck's constant, k_B is the Boltzmann constant and $\Delta\nu_c$ is the peak separation in Hz at coalescence.[39]

[a] The peak separation $\Delta\nu_c$ was obtained by a least-squares plot of $\Delta\nu$ and temperature and extrapolation to T_c using the $^{31}P\{^1H\}$ NMR data.[40]

[b] The peak separation $\Delta\nu_c$ was obtained directly from the appropriate low temperature spectra.[39]

CONCLUSIONS

A new, second generation ligand system has been developed and its coordination chemistry with zirconium(IV) examined. The versatile mononuclear trichloride derivative $[P_2Cp]ZrCl_3$ **1** has been prepared and from it, the formation of a series of hydrocarbyl complexes of the formula $[P_2Cp]ZrCl_{3-x}R_x$ (R = Me or CH_2Ph; $x = 1$ or 3) has been investigated. What emerges from this study is that coordination of the pendant phosphine arms becomes less favorable as the number of alkyl substituents increases. Even the introduction of one bulky hydrocarbyl substituent at zirconium is enough to increase the tendency for phosphine dissociation such that the low temperature limiting structure is five-coordinate. A further consequence of this reduced tendency for phosphine binding is that fluxional processes become prevalent; the fluxional behavior of these complexes is also dependent on the number and size of the hydrocarbyl substituents.

EXPERIMENTAL

General information

All manipulations were performed under prepurified nitrogen in a Vacuum Atmospheres HE-

553-2 glovebox equipped with a MO-40-2H purification system or in standard Schlenk-type glassware on a dual vacuum/nitrogen line. Hexanes and tetrahydrofuran (THF) were initially dried over CaH_2 followed by distillation from sodium-benzophenone ketyl under argon. Ether and toluene were distilled from sodium-benzophenone ketyl. The deuterated solvents C_6D_6 and $C_6D_5CD_3$ were dried overnight with activated 4 Å molecular sieves, vacuum transferred to an appropriate container, "freeze–pump–thawed" three times and stored in the glovebox. Carbon, hydrogen and nitrogen analyses were performed by Mr P. Borda of this department; repeated attempts to obtain elemental analyses of the hydrocarbyl zirconium complexes were unsuccessful, presumably because the materials are oils. NMR spectra were recorded in C_6D_6 unless otherwise stated. ^1H NMR spectra (referenced to C_6D_5H at 7.15 ppm or $C_6D_5CD_2H$ at 2.09 ppm) were performed on one of the following instruments depending on the complexity of the particular spectrum: Bruker WH-200, Varian XL-300, Bruker WH-400 or a Bruker AM-500. ^{13}C NMR spectra (referenced to C_6D_6 at 128.0 ppm or $C_6D_5CD_3$ at 20.4 ppm) were run at 75.429 MHz ($^1J_{C-H}$ coupling constants are reported in square brackets) and ^{31}P NMR spectra (referenced to external $P(OMe)_3$ in C_6D_6 or $C_6D_5CD_3$ at 141.0 ppm) were run at 121.421 MHz, both on the XL-300. All chemical shifts are reported in ppm and all coupling constants are reported in Hz. The preparation of [P$_2$Cp]Li = (η^5-C_5H_3-1,3-($SiMe_2CH_2P Pr^i_2$)$_2$)Li will be reported separately.[34]

Preparation of [P$_2$Cp]ZrCl$_3$

To a slurry of $ZrCl_4(THT)_2$ (6.141 g, 15.00 mmol) in toluene (130 cm^3) was added a toluene solution (100 cm^3) of [P$_2$Cp]Li {[P$_2$Cp]Li = (η^5-C_5H_3-1,3-($SiMe_2CH_2PPr^i_2$)$_2$)Li} (6.731 g, 15.00 mmol) dropwise over 10 min. After 12 h the toluene solution was filtered through Celite to remove LiCl. The toluene was removed under vacuum, and the solid was pumped for 3 h to remove all the THT. The crystals were washed with hexanes (three times) and pumped to dryness to give 8.91 g (93% yield) of pale yellow, diamond-shaped crystals. Anal. found: C, 42.94; H, 7.46; anal. calc. for $C_{23}H_{47}Cl_3P_2Si_2Zr$: C, 43.21; H, 7.41. ^1H NMR: 0.16 (s, 6H, $Si(CH_3)_2$), 0.39 (s, 6H, $Si(CH_3)_2$), 0.75 (d, $J = 3$ Hz, 2H, $SiCH_2P$), 0.85 (d, $J = 3$ Hz, 2H, $SiCH_2P$), 1.07 (m, 12H, $CH(CH_3)_2$), 1.25 (m, 12H, $CH(CH_3)_2$), 2.08 (sept., 2H, $CHMe_2$), 2.65 (sept., 2H, $CHMe_2$), 6.73 (d, $J = 1.6$ Hz, 2H, C_5H_3), 7.30 (t, $J = 1.6$ Hz, 1H, C_5H_3). $^{31}P\{^1H\}$ NMR: 10.69 (s). $^{13}C\{^1H\}$ NMR: 128.2 (s, C_5H_3), 126.8 (s, C_5H_3), 26.4 (d of d, $CH(CH_3)_2$), 24.9 (d of d, $CH(CH_3)_2$), 19.6 (s, $CH(CH_3)_2$), 18.9 (s, $CH(CH_3)_2$), 18.77 (s, $CH(CH_3)_2$), 18.67 (s, $CH(CH_3)_2$), 8.81 (m, $SiCH_2P$), 0.06 (d, $J = 1.2$ Hz, $Si(CH_3)_2$), 0.02 (d, $J = 1.2$ Hz, $Si(CH_3)_2$), −1.00 (d, $J = 1.9$ Hz, $Si(CH_3)_2$), −1.04 (d, $J = 1.9$ Hz, $Si(CH_3)_2$).

Preparation of [P$_2$Cp]Zr(CH$_2$Ph)$_3$

To a cooled (−78 °C) toluene solution (50 cm^3) of [P$_2$Cp]ZrCl$_3$ (100 mg, 0.156 mmol) was added a toluene solution (7 cm^3) of $Mg(CH_2Ph)_2 \cdot 2THF$ (81.9 mg, 0.233 mmol) dropwise. The pale yellow color of the [P$_2$Cp]ZrCl$_3$ solution immediately became orange. The solution was allowed to slowly warm to room temperature. All the volatiles were then removed under vacuum and the residue was extracted with hexanes, filtered and the solvent was removed under vacuum, to give a yellowish oil. Spectroscopic data established the stoichiometry of the compound. ^1H NMR: 7.11 (t, $J = 7.4$ Hz, meta H, 6H, C_6H_5), 6.93 (t, $J = 7.3$ Hz, para H, 3H, C_6H_5), 6.68 (d, $J = 7.5$ Hz, ortho H, C_6H_5), 6.96 (t, $J = 1.8$ Hz, 1H, C_5H_3), 6.40 (d, $J = 1.8$ Hz, 2H, C_5H_3), 1.86 (s, 6H, CH_2Ph), 1.53 (d of sept, $J_{H-H} = 7.0$ Hz, $J_{H-P} = 3.3$ Hz, 4H, $CHMe_2$), 0.96 (m, 24H, $CH(CH_3)_2$), 0.58 (d, $J = 3.5$ Hz, 4H, $SiCH_2P$), 0.36 (s, 12H, $Si(CH_3)_2$). $^{31}P\{^1H\}$ NMR: −5.20 (s). $^{13}C\{^1H\}$ NMR: 144.9 (s, para C_6H_5), 129.8 (s, meta C_6H_5), 128.9 (s, ortha C_6H_5), 124.28 (two doublets, $J = 1.8$ Hz, Cp1, Cp3), 123.56 (s, Cp4, Cp5), 123.36 (s, Cp2), 69.25 (s, $ZrCH_2Ph$), 25.19 (d, $J = 14.8$ Hz, $CHMe_2$), 24.85 (d, $J = 16.8$ Hz, $CHMe_2$), 20.0 (d, $J = 5.8$ Hz, $2CH(CH_3)_2$), 19.72 (d, $J = 5.1$ Hz, $CH(CH_3)_2$), 19.10 (d, $J = 11.4$ Hz, $CH(CH_3)_2$), 7.66 (d, $J = 39.9$ Hz, $SiCH_2P$), −0.12 (d, $J = 5.6$ Hz, $Si(CH_3)_2$).

Preparation of [P$_2$Cp]ZrCl$_2$(CH$_2$Ph)

To a cooled (−78 °C) toluene solution (50 cm^3) of [P$_2$Cp]ZrCl$_3$ (100 mg, 0.156 mmol) was added a toluene solution (7 cm^3) of $Mg(CH_2Ph)_2 \cdot 2THF$ (27.3 mg, 0.078 mmol) dropwise. The pale yellow color of the [P$_2$Cp]ZrCl$_3$ solution immediately became orange. The mixture was allowed to slowly warm to room temperature and then stirred at this temperature for 12 h; all of the volatiles were then removed under vacuum and the residue extracted with hexanes. The hexanes solution was filtered and the solvent removed under vacuum to give a yellowish oil. Spectroscopic data established the stoichiometry of the compound. ^1H NMR: 7.55 (d, $J = 7.5$ Hz, 2H, C_6H_5), 7.32 (t, $J = 7.5$ Hz, 2H, C_6H_5), 7.15 (t, $J = 7.6$ Hz, 1H, C_6H_5), 6.54 (d, $J = 1.7$ Hz, 2H, C_5H_3), 2.9 (broad s, 2H, CH_2Ph),

2.36 (m, 4H, C*H*Me$_2$), 0.97 (m, 24H, CH(C*H*$_3$)$_2$),0.93 (d, J = 3.6 Hz, 4H, SiC*H*$_2$P), 0.44 (s, 12H, Si(C*H*$_3$)$_2$). ^{31}P{^{1}H} NMR: coalescence at 30°C, 5.8 ppm (s) (70°C). ^{13}C{^{1}H} NMR: 146.8 (s, para *C*$_6$H$_5$), 130.3 (s, meta *C*$_6$H$_5$), 127.9 (s, ortho *C*$_6$H$_5$), 126.1 (s, Cp4 or Cp5), 123.5 (s, Cp5 or Cp5), 121.6 (s, Cp2), 75.7 (t, J = 8.6 Hz, Zr*C*H$_2$Ph), 25.7 (d, J = 19.4 Hz, *C*HMe$_2$), 25.6 (d, J = 20.7 Hz, *C*HMe$_2$), 19.5 (d, J = 5.8 Hz, CH(*C*H$_3$)$_2$), 19.1 (d, J = 5.1 Hz, CH(*C*H$_3$)$_2$), 18.4 (d, J = 9.0 Hz, CH(*C*H$_3$)$_2$), 9.8 (broad peak, coalescence, Si*C*H$_2$P), −0.31 (d, J = 3.6 Hz, Si(*C*H$_3$)$_2$), −1.18 (d, J = 5.8 Hz, Si(*C*H$_3$)$_2$).

Preparation of [P$_2$Cp]Zr(CH$_3$)$_3$

To a cooled (−78°C) toluene solution (50 cm^3) of [P$_2$Cp]ZrCl$_3$ (1.00 g, 1.56 mmol) was added a toluene/THF solution (3.91 cm^3) of Mg(CH$_3$)Br (1.4 M, 5.47 mmol) dropwise over 10 min. The solution was warmed to ambient temperature. After stirring for 12 h the toluene was removed under vacuum and the residue was extracted with hexanes (2 × 25 cm^3). The white solid (MgBrCl) was filtered off through Celite. The hexanes were removed under vacuum to give 0.6 g (70%) of the trimethyl complex as a yellowish oil. Spectroscopic data established the stoichiometry of the compound. ^{1}H NMR: 0.37 (s, 12H, Si(C*H*$_3$)$_2$), 0.54 (t, J = 2.8 Hz, 9H, Zr(C*H*$_3$)$_3$), 0.70 (d, J = 6.5 Hz, 4H, SiC*H*$_2$P), 1.0 (m, 24H, CH(C*H*$_3$)$_2$), 1.6 (d of septet, J_{P-H} = 3.1, J_{H-H} = 7.2 Hz, 4H, C*H*Me$_2$), 6.42 (t, J = 1.9 Hz, 1H, C$_5$*H*$_3$), 6.71 (d, J = 1.9 Hz, 2H, C$_5$*H*$_3$). ^{13}C{^{1}H} NMR: 125.35 (d, J = 3.8 Hz, Cp1, Cp3), 121.88 (d, Cp4, Cp5), 121.45 (t, Cp2), 42.74 (t, J = 2.6 Hz, Zr*C*H$_3$), 25.74 (d, J = 7.4 Hz, *C*HMe$_2$), 25.68 (d, J = 7.9 Hz, *C*HMe$_2$), 19.55 (d, J = 8.8 Hz, 2CH(*C*H$_3$)$_2$), 19.36 (d, J = 8.3 Hz, CH(*C*H$_3$)$_2$), 19.21 (d, J = 6.7 Hz, CH(*C*H$_3$)$_2$), 10.34 (d, J = 23.8 Hz, Si*C*H$_2$P), −0.16 (d, J = 4.1 Hz, Si(*C*H$_3$)$_2$), −0.63 (d, J = 5.4 Hz, Si(*C*H$_3$)$_2$). ^{31}P{^{1}H} NMR: 2.3 (s).

X-ray crystallographic analysis of [P$_2$Cp]ZrCl$_3$

Crystallographic data appear in Table 7. The final unit-cell parameters were obtained by least-squares on the setting angles for 25 reflections with 2θ = 20.0–34.8°. The intensities of three standard reflections, measured every 200 reflections throughout the data collection, showed only small random fluctuations. The data were processed[42] and corrected for Lorentz and polarization effects, and absorption (empirical, based on azimuthal scans for three reflections).

The structure was solved by conventional heavy atom methods, the coordinates of the Zr, P, and Si atoms being determined from the Patterson function and those of the remaining atoms from subsequent difference Fourier syntheses. All non-hydrogen atoms were refined with anisotropic thermal parameters. Hydrogen atoms were fixed in calculated positions (staggered methyl groups, C—H = 0.98 Å, B_H = 1.2 $B_{\text{bonded atom}}$). No correction for secondary extinction was indicated. A parallel refinement of the mirror-image structure

Table 7. Crystallographic data for [P$_2$Cp]ZrCl$_3$[a]

Compound	[P$_2$Cp]ZrCl$_3$
Formula	C$_{23}$H$_{47}$Cl$_3$P$_2$Si$_2$Zr
Formula weight	639.32
Color, habit	Pale yellow, prism
Crystal size (mm)	0.15 × 0.15 × 0.40
Crystal system	Orthorhombic
Space group	$P2_12_12_1$
a (Å)	14.282(2)
b (Å)	15.877(3)
c (Å)	13.791(3)
V (Å^3)	3127.1(9)
Z	4
D_{calc} (g cm^{-3})	1.358
F(000)	1336
μ(Mo-K_α) (cm^{-1})	7.91
Transmission factors (relative)	0.93–1.00
Scan type	ω–2θ
Scan range (deg in ω)	1.10 + 0.35 tan θ
Scan speed (deg min^{-1})	16
Data collected	$+h$, $+k$, $+l$
$2\theta_{max}$ (°)	60
Crystal decay (%)	Negligible
Total reflections (all unique)	5069
Reflections with $I > 3\sigma(I)$	2907
No. of variables	280
R	0.032
R_w	0.027
GOF	1.34
Max Δ/σ (final cycle)	0.002
Residual density (e Å^{-3})	−0.33, 0.39 (both near Zr)

[a] Temperature 294 K, Rigaku AFC6S diffractometer, Mo-K_α (λ = 0.71069 Å) radiation, graphite monochromator, takeoff angle 6.0°, aperture 6.0 × 6.0 mm at a distance of 285 mm from the crystal, stationary background counts at each end of the scan (scan/background time ratio 2:1), $\sigma^2(F^2) = [S^2(C+4B)]/Lp^2$ (S = scan rate, C = scan count, B = normalized background count), function minimized $\Sigma w(|F_o| - |F_c|)^2$ where $w = 4F_o^2/\sigma^2(F_o^2)$, $R = \Sigma||F_o| - |F_c||/\Sigma|F_o|$, $R_w = (\Sigma w(|F_o| - |F_c|)^2/\Sigma w|F_o|^2)^{1/2}$, and GOF = $[\Sigma w(|F_o| - |F_c|)^2/(m-n)]^{1/2}$. Values given for R, R_w, and GOF are based on those reflections with $I > 3\sigma(I)$.

resulted in higher residuals: the R and R_w factor ratios are 1.037 and 1.023, respectively. Neutral atom scattering factors for all atoms and anomalous dispersion corrections for the non-hydrogen atoms were taken from the *International Tables for X-Ray Crystallography*.[43] Selected bond lengths and bond angles appear in Tables 1 and 2, respectively. Final atomic coordinates and equivalent isotropic thermal parameters, hydrogen atom coordinates and thermal parameters, anisotropic thermal parameters, complete tables of bond lengths and angles, torsion angles, intermolecular contacts, and least-squares planes are included as supplementary material.

Acknowledgments—Financial support was provided by NSERC of Canada in the form of operating grants. We also thank Professor R. H. Morris for a copy of his Macintosh version of D-NMR5. In addition, the comments of a referee are gratefully acknowledged.

Supplementary material available—Final atomic coordinates and equivalent isotropic thermal parameters, hydrogen atom coordinates and thermal parameters, anisotropic thermal parameters, complete tables of bond lengths and angles, torsion angles, intermolecular contacts, and least-squares planes, measured and calculated structure factor amplitudes for $[P_2Cp]ZrCl_3$ (35 pages).

REFERENCES

1. J. Okuda, *Angew. Chem., Int. Ed. Engl.* 1992, **31**, 47.
2. W. Kaminsky, A. Bark and R. Steiger, *J. Mol. Catal.* 1992, **74**, 109.
3. W. Kaminsky and H. Sinn (Eds), *Transition Metals and Organometallics as Catalysts for Olefin Polymerization*. Springer, New York (1988).
4. W. Kaminsky, K. Külper, H.-H. Brintzinger and F. R. W. P. Wild, *Angew. Chem., Int. Ed. Engl.* 1985, **24**, 507.
5. R. F. Jordan, C. S. Bajgur, R. Willer and B. J. Scott, *J. Am. Chem. Soc.* 1986, **108**, 7410.
6. J. C. W. Chien, W. M. Tsai and M. D. Rausch, *J. Am. Chem. Soc.* 1991, **113**, 8570.
7. J. C. W. Chien and R. J. Sugimoto, *J. Polym. Sci., Part A* 1991, **29**, 459.
8. W. Kaminsky, A. Ahlers and N. Möller-Lindenhof, *Angew. Chem., Int. Ed. Engl.* 1989, **28**, 1216.
9. P. Pino, P. Cioni and J. Wei, *J. Am. Chem. Soc.* 1987, **109**, 6189.
10. R. F. Jordan, E. D. William and S. F. Echols, *J. Am. Chem. Soc.* 1986, **108**, 1718.
11. R. F. Jordan, R. E. LaPointe, C. S. Bajgur, S. F. Echols and R. Willet, *J. Am. Chem. Soc.* 1987, **109**, 4111.
12. D. T. Mallin, M. D. Rausch, Y.-G. Lin, S. Dong and J. C. W. Chien, *J. Am. Chem. Soc.* 1990, **112**, 2030.
13. R. F. Jordan, P. K. Bradley, N. C. Baenziger and R. E. LaPointe, *J. Am. Chem. Soc.* 1990, **112**, 1289.
14. R. Taube and L. Krukowka, *J. Organomet. Chem.* 1988, **347**, C9.
15. X. Yang, C. L. Stern and T. J. Marks, *J. Am. Chem. Soc.* 1991, **113**, 3623.
16. X. Yang, C. L. Stern and T. J. Marks, *Organometallics* 1991, **10**, 840.
17. G. G. Hlatky, H. W. Turner and R. R. Eckman, *J. Am. Chem. Soc.* 1989, **111**, 2728.
18. G. G. Hlatky, R. R. Eckman and H. W. Turner, *Organomet. Syn.* 1992, **11**, 1413.
19. M. Bochmann, A. J. Jaggar and J. C. Nicholls, *Angew. Chem., Int. Ed. Engl.* 1990, **29**, 780.
20. M. Bochmann and A. J. Jaggar, *J. Organomet. Chem.* 1992, **424**, C5.
21. M. Bochmann, S. J. Lancaster, M. B. Hursthouse and K. M. A. Malik, *Organometallics* 1994, **13**, 2235.
22. E. B. Coughlin and J. E. Bercaw, *J. Am. Chem. Soc.* 1992, **114**, 7606.
23. W. Kaminsky, K. Kulper, H.-H. Brintzinger and F. R. W. P. Wild, *Angew. Chem., Int. Ed. Engl.* 1985, **24**, 507.
24. G. Rieger and J. C. W. Chien, *Polym. Bull.* 1989, **21**, 159.
25. G. Rieger, X. Mu, D. T. Mallin, M. D. Rausch and J. C. W. Chien, *Macromolecules* 1990, **23**, 3559.
26. J. A. Ewen, L. Haspeslagh, J. L. Atwood and H. Zhang, *J. Am. Chem. Soc.* 1987, **109**, 6544.
27. J. A. Ewen, R. L. Jones, A. Razavi and J. D. Ferrara, *J. Am. Chem. Soc.* 1988, **110**, 6255.
28. H. Schnutenhaus and H.-H. Brintzinger, *Angew. Chem., Int. Ed. Engl.* 1979, **18**, 777.
29. R. L. Halterman, *Chem. Rev.* 1992, **92**, 965.
30. M. D. Fryzuk, *Can. J. Chem.* 1992, **70**, 2839.
31. M. D. Fryzuk, T. S. Haddad, D. J. Berg and S. J. Rettig, *Pure Appl. Chem.* 1991, **63**, 845.
32. R. E. Dessy, Y. Okuzumi and A. Chen, *J. Am. Chem. Soc.* 1962, **84**, 2899.
33. R. R. Fraser and T. S. Mansour, *J. Org. Chem.* 1984, **49**, 5284.
34. M. D. Fryzuk, S. S. H. Mao, M. J. Zaworotko and L. R. MacGillivray, *J. Am. Chem. Soc.* 1993, **115**, 5336.
35. M. D. Fryzuk, A. Carter and A. Westerhaus, *Inorg. Chem.* 1985, **24**, 642.
36. L. M. Engelhardt, R. I. Papasergio, C. L. Raston and A. H. White, *Organometallics* 1984, **3**, 18.
37. A. Bondi, *J. Phys. Chem.* 1964, **68**, 441.
38. P. T. Wolczanski and J. E. Bercaw, *Organometallics* 1982, **1**, 793.
39. W. A. Thomas, *Annu. Rev. NMR Spectrosc.* 1968, **1**, 43.
40. See ref. 18 in M. D. Fryzuk and P. A. MacNeil, *J. Am. Chem. Soc.* 1984, **106**, 6993.
41. M. D. Fryzuk, A. Carter and S. J. Rettig, *Organometallics* 1992, **11**, 469.
42. TEXSAN/TEXRAY structure analysis package (Molecular Structure Corp., 1985).
43. *International Tables for X-Ray Crystallography*, Vol. IV, pp. 99–102, 149. Kynoch Press, Birmingham U.K. (present distributor Kluwer Academic Publishers, Dordrecht, The Netherlands) (1974).